Korean J. Chem. Eng., 39(7), 1673-1687 (2022)
DOI: 10.1007/s11814-022-1151-y

pISSN: 0256-1115
eISSN: 1975-7220

Study of gradual and sudden operating condition variations to optimize energy and mass consumption of an industrial fluidized catalytic cracking (FCC) unit with a high-efficiency regenerator

Khashayar Yaghoubi*, Neda Gilani,†, Sorood Zahedi Abghari***,†, Farangis Fallah Mehneh*, and Mohammad Eisazadeh******

*Fouman Faculty of Engineering, College of Engineering, University of Tehran, P. O. Box, Fouman 43516-66456, Iran
**Department of Chemical Engineering, University of Guilan, Rasht 41996-13776, Iran
***Refinery Technology Development Department, Research Institute of Petroleum Industry (RIPI), Tehran 1485613111, Iran
****Process Engineering Department, Abadan Refinery, Abadan 6316915651, Iran
(*Received 20 August 2021 • Revised 28 March 2022 • Accepted 19 April 2022*)

Abstract−A dynamic model was developed to investigate the impact of operating conditions on the main output variables of the fluidized catalytic cracking (FCC) process with a high-efficiency regenerator and to determine the optimal amounts of operating variables, at the Abadan refinery FCC unit in Iran. To determine the rate constants in the developed kinetic model and other related constants in the developed model, a wide range of industrial data were gathered from the targeted process over several months. Through applying an adjusted dynamic model, the effect of gradual increases in feed preheat temperature (350-500 K) on the yield of gasoline and LCO was investigated, and increases in both yields were observed. The effects of sudden changes in feed preheat temperature, feed and regenerated catalyst flow rate on gasoline yield were also examined. The results showed that a sudden 6.9% increase in feed, a sudden 30 K decrease in temperature and a sudden 1.12% decrease in catalyst flow rate resulted in 2%, 0.27% and 0.5% decreases in gasoline, respectively. Furthermore, potential methods for neutralizing these negative effects on the gasoline yield were investigated. Finally, the operating conditions were optimized to improve the gasoline and octane number. Three different optimization cases were studied. The profitability of the unit increased about $2.5-3.8 million per year. A reduction in energy consumption of 12,500 to 21,000 Gj/yr was achieved. The amount of feed and the catalyst flow rate were also decreased by 1.5% and 0.2%-0.9%, respectively.

Keywords: Fluid Catalytic Cracking, Dynamic Modeling, Optimization, High-efficiency Regenerator, Abadan Refinery

INTRODUCTION

One of the most vital upgrading refinery processes designed to produce light products, such as gasoline and LPG, is the fluidized catalytic cracking (FCC) process. The riser reactor and the regenerator are the two key parts of this process; the riser reactor is the equipment in which the cracking reactions network occurs and, in the regenerator, the deactivated catalyst is regenerated. Indeed, the coke formed on the active sites of the catalyst is burned through blowing fresh air from the bottom of the regenerator (called combustor section) and eventually the catalyst is regenerated by conducting the combustion reactions. The main product of the FCC unit is gasoline; about 45% of the world gasoline is produced by this process and its subsidiary processes [1].

The modeling of FCC units has been studied since 1970. The pioneering study in this field was conducted by Weekman and Nace in 1970, in which a three-lump kinetic network was developed and implemented to model the reactions and estimate the distribution yields of different products [2]. The additional three to five-lump models were also proposed by other researchers [3-14] Subsequently, a new six-lump kinetic scheme considering the cracking of LPG to coke, dry gas and the cracking of dry gas into coke was developed [15]. An eight-lump kinetic model that included VGO, gasoline, LPG, butylene, propylene, ethylene, light gases and coke was presented [16].

In the majority of FCC modeling studies, the regenerator has been considered as having a two-phase section (bubble and emulsion), in which the bubble phase is rich in gas and the emulsion phase is rich in the catalyst. Few studies were observed on units with a high-efficiency regenerator. The riser dynamic behavior simulation and models with an adiabatic mode assumption for the riser have been conducted and were presented considering two phases for the regenerator [17-19]. Another model presented for the FCC unit in dynamic conditions considered the riser as a plug flow reactor that made no correct predictions of the CO_2/CO ratio [20]. In another study, a dynamic modeling and simulation of a FCC process was presented and structural analysis was performed in order to investigate observability of the system [21]. In addition to the riser-reactor and regenerator, the modeling of catalyst transfer lines was performed, where momentum equations, along with mass and energy equations, were considered. However, since the FCC unit is

†To whom correspondence should be addressed.
E-mail: n.gilani@guilan.ac.ir, gilani.chem@gmail.com, zahedis@ripi.ir

very complex, this model, in addition to its high precision, is not suitable for industrial use [22].

A simulation of an FCC riser with a variable diameter was performed and the results showed more gasoline yield [23]. Fernandes et al. provided a dynamic model including the riser, stripper, regenerator and catalyst transfer lines using a six-lump kinetic network that had been presented in the work of other researchers, in which the riser was considered as a plug flow reactor [24,25]. In the following, a high-efficiency regenerator designed by UOP that was divided into three sections (i.e., combustor, lift and regenerator) was modeled with more details to analyze the multiplicity of steady states [26,27]. Moreover, different catalytic deactivation models were investigated in terms of their effects on a dynamic model of the high-efficiency regenerator of an industrial FCC unit designed by UOP [28]. The model presented in their study was similar to the model presented by these authors in 2006 and 2007. However, in this work, the dilute phase in the regenerator (called the freeboard), was also modeled so that the regenerator was divided into two phases (i.e., the dense phase and the dilute phase), wherein the dense phase was assumed to be a CSTR reactor and the dilute phase was modeled as plug flow [25,26].

The unit optimization and the investigation of the effect of the operating conditions were performed, such as implementing an optimization process system for the FCC unit using a sequential quadratic programming (SQP) method. The results showed that, if the process works in full combustion, it will increase cost savings and operating profits [29].

Furthermore, the effect of operating conditions on the multiplicity of steady states for the FCC unit was investigated. The results showed that operating conditions cannot be manipulated to change the number of steady states [30]. To maximize the FCC unit performance, models for unit optimization were presented in which the model optimization was based on product maximization by specifying operating conditions, including mass flows and inlet temperatures. This type of optimization was effective in determining the optimum operating conditions for maximum production, but it did not take into account the amount of energy needed to produce the desired products and the additional investment required [31,32].

In this context, a dynamic optimizer for an industrial FCC unit that was developed by performing a numerical analysis and employing a dynamic mechanical model was also investigated [33]. Estimations were given for the kinetic parameters via non-linear optimization method. The optimum coke value obtained was lower than that reported in previous studies. They also investigated the effect of temperature on VGO conversion. Their results showed that the conversion of VGO increased at high temperatures [34]. The effect of FCC severity on the concentration profiles of products was investigated and the effects of operating conditions on various olefins detailed distribution were discussed [16].

Moreover, to curb the research octane number (RON) loss, an optimization was carried out on a FCC refining process. In this case, the random forest-based feature selection algorithm was used to select the main variables, then a hybrid grey wolf optimizer algorithm was employed to minimize RON loss under the appropriate constraints [35].

Many research octane number (RON) and products yield improvements have been achieved through catalyst development. For example, this has been done by adding or reducing some elements to the catalyst of the FCC unit (e.g., vanadium and mordenite) or by changing the acid/metal balance of the catalyst in the unit. The results showed that adding these materials increases activity and selectivity for gasoline. Furthermore, the change in the acid/metal catalyst balance in addition to the octane number also affects the liquid yield [36-41]. Also, a bilayer catalyst constituted of amorphous silica-alumina layer coated on Y zeolite layer was applied as a catalyst of FCC unit that increased benzene and toluene yield and reduced coke formation [42].

In the present study, the Abadan refinery FCC unit was modeled dynamically for a case study, the results of which have been validated by the industrial plant data. Subsequently, the estimates of kinetic constants were investigated with the aim of achieving more precise responses to unit data. The effects of turbulence in operating conditions, including the effect of gradual increases in feed preheat temperature on the yield of gasoline and LCO, were investigated. Furthermore, the effects of sudden changes in feed preheat temperature, feed flow rate and regenerated catalyst flow rate on the yield of gasoline were also investigated, with suggestions given on how to neutralize these effects using a dynamic model that have not been investigated in the previous studies. Moreover, an optimization process aimed at increasing the gasoline yield, reduce energy consumption, improve the RON and increase unit profitability was presented. In the current study, RON improvement was performed through optimising the operating conditions.

PROCESS DESCRIPTION

The FCC unit is one of the most important refineries in which the heavy feed, the output gasoil from the vacuum column, converts to lighter and more valuable products, such as gasoline, LPG, LCO and dry gas. In addition, coke is produced due to the burning of hydrocarbons. The main equipment of the unit consists of the riser reactor operating at about 793.15 K and the regenerator at a temperature of about 1,013.15 K.

There are two different configurations for the FCC unit: stack type and the side-by-side type, of which is one of this kind of design type is a side-by-side FCC unit with high-efficiency regenerator. Fig. 1 and Fig. 2 represent these two types of design for the FCC unit. The high-efficiency UOP regenerator design was introduced in the late 1970s, which minimizes the inherent problems of blending in bubble bed regenerators [43]. The main difference between these types of design with the previous designs is in removing the bubble substrate. In older designs, the regenerators had two regions, the emulsion and the bubble phases, but high-efficiency regenerators consist of the dense bed and the freeboard.

High-efficiency regenerators are divided into three parts. The combustor, in which the burning air enters from this section and is mixed with the spent catalyst from the reactor and the recirculated catalyst, the lift section, which moves the catalysts from combustor to the regenerator vessel, and the regenerator, in which burning gases are separated from the catalyst and form a dense bed [27].

The FCC catalysts are in the form of fine powder particles made of silica-alumina with an average particle size 75-85 μm.

The hot fresh catalyst and VGO as feed (after atomizing) simultaneously enter the riser. Hydrocracking reactions immediately happen after feed and catalyst contact, so that most reactions occur at the beginning of the riser at about a few seconds. Then, catalysts are spent in order to reactivate the move to the regenerator through the catalyst transport line.

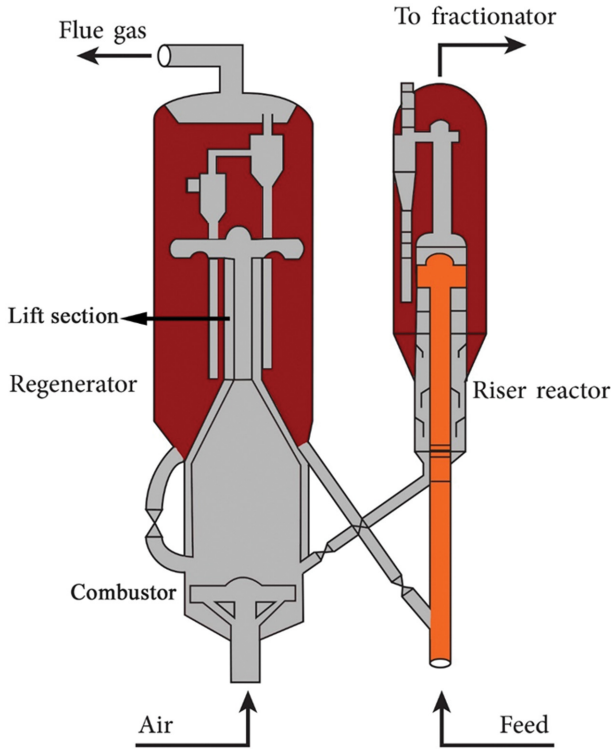

Fig. 1. FCC unit with high-efficiency regenerator.

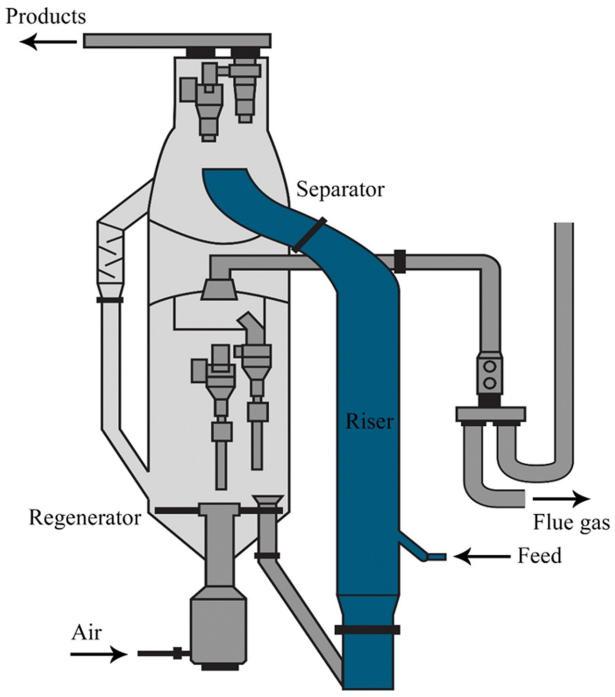

Fig. 2. FCC unit with stack design.

In the high-efficiency regenerator, combustion air is used to burn the coke on the catalyst. Coke burning operations continue along the lift section and, after reaching the regenerator, catalysts collapse and form a dense bed. Note that most of the coke is burned in the combustor and lift section. In the lower part of the combustor, it is assumed that just mixing the burning air and the catalyst flows (spent catalyst and recirculated catalyst flows) occurs without any combustion reactions, and most of the burning reactions occur in the upper part of the combustor and the lift section [27]. To burn the remaining coke in the regenerator, the fluffing air enters the bottom of the regenerator to form the fluidized bed and burn the coke; however, this coke burning is to a very low extent compared to the burning in the combustor and lift section. After the coke is burned, the regenerated catalysts return to the riser. Gases go to the freeboard section and then, after reaction between CO and O_2, the flue gas exits from above the freeboard section.

MODELING

Models of the two main equipment of the Abadan refinery FCC unit, riser reactor and high-efficiency regenerator are presented in this section.

1. Riser

The plug flow assumption is considered to model the riser reactor. In addition, a six-lump kinetic model is fully implemented to consider the reactions that occur in the reactive mixture. The applied pseudo lumps are VGO, LCO, GLN, LPG, FG and coke [22,44]. The pseudo-reaction network is illustrated in Fig. 3. All the reaction rates are first order, except VGO cracking reactions.

The rate of reaction of lump i toward lump j is calculated by Eq. (1):

$$r_{ij} = \varphi A_{ij} \exp\left(-\frac{E_{ij}}{RT_{rs}}\right) \hat{C}_i^{n_{ij}} \quad (1)$$

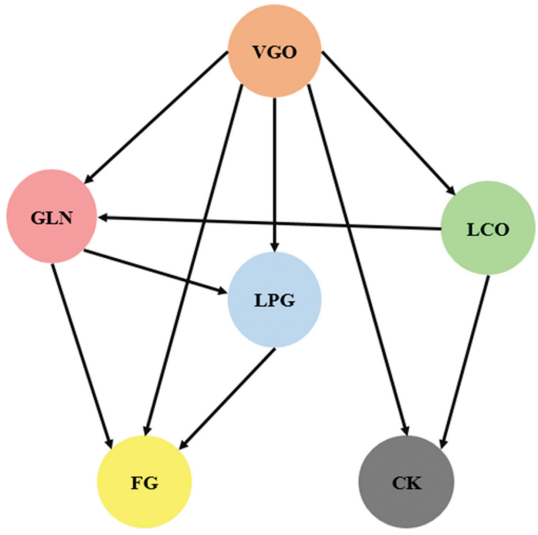

Fig. 3. Kinetic scheme of the cracking reactions occurring in the rise.

where φ is catalyst deactivation function, which is calculated by the following empirical equation:

$$\varphi = \exp(-\alpha_c Y_{ck}^{cat}) \tag{2}$$

The following correlation demonstrates the governing mass balance equation for each lump and the coke:

$$\frac{\partial x_i}{\partial t} = -\frac{F_{tf}}{\varepsilon_g A_{rs} \rho_{ov}} \frac{\partial x_i}{\partial z} + r_i \tag{3}$$

where x_i is weight fraction of the feed, products and coke, t is time, and z is the axial coordinate. F_{tf}, ρ_{ov} and A_{rs} are feed mass flow rate, feed density as vapor (the feed atomises before entering to the riser) and riser cross-sectional, respectively.

The energy balance for the riser is according to the following correlation:

$$\rho_m C_{p_m} \frac{\partial T_{rs}}{\partial t} + \frac{F_g C_{p_g} + F_c C_{p_c}}{A_{rs}} \frac{\partial T_{rs}}{\partial z} = \varepsilon_c \Delta H_{crk} r_{VGO} \tag{4}$$

where ρ_m and C_{p_m} are mean density and average heat capacity of components in the riser, respectively.

2. High-efficiency Regenerator

Coke is considered to be mainly composed of carbon and hydrogen when it comes to burning kinetics in the high-efficiency regenerator. There is also sulfur and nitrogen; however, they can be ignored due to their insignificance. Therefore, only the burning of carbon and hydrogen is considered [27].

The main reactions that occur in the regenerator are as follows:

$$C + \frac{1}{2}O_2 \xrightarrow{r_1^s} CO \tag{5}$$

$$C + O_2 \xrightarrow{r_2^s} CO_2 \tag{6}$$

$$H + \frac{1}{4}O_2 \xrightarrow{r_3^s} \frac{1}{2}H_2O \tag{7}$$

$$CO + \frac{1}{2}O_2 \xrightarrow{r_4^s} CO_2 \tag{8}$$

$$CO + \frac{1}{2}O_2 \xrightarrow{r_5^g} CO_2 \tag{9}$$

Carbon combustion reactions simultaneously produce CO and CO_2. CO to CO_2 oxidation can occur in heterogeneous (catalytic) and homogeneous states [26]. The following equations present the rate of each reaction [45-47]:

$$r_1^s = r_c\left(\frac{1}{1+\sigma}\right) \tag{10}$$

$$r_2^s = r_c\left(\frac{\sigma}{1+\sigma}\right) \tag{11}$$

$$r_3^s = k_3^s \exp\left(-\frac{E_{a3}^s}{RT}\right) P_{O_2} Y_H \tag{12}$$

The rates of CO combustion in heterogeneous and homogeneous conditions are according to following equations:

$$r_4^s = k_4^s \exp\left(-\frac{E_{a4}^s}{RT}\right) P_{O_2}^{0.5} P_{CO}^{0.49} P_{H_2O}^{-0.26} \tag{13}$$

$$r_1^g = \frac{k_1^g \exp\left(-\frac{E_{a1}^g}{RT}\right)}{T^{2.1}} y_{O_2}^{0.6} y_{CO} y_{H_2O}^{0.5} \tag{14}$$

The combustor can be divided into two parts: the lower part and the upper part. The lower part is where mixing the catalyst flows and the entering air occurs, while the upper part is where the combustion reactions occur and will then continue in the lift section.

The upper part of the combustor and lift section was modeled as a plug flow reactor and most of the reactions occur there. Mass and energy balances for the combustor and the lift section are according to the following equations [27]:

Molar balance for gaseous species:

$$\frac{\partial N_{iLF}^g}{\partial z} = A_{LF}(\varepsilon_{gLF} \Sigma_j (r_j^g \vartheta_{ji}^g) + \varepsilon_{cLF} \rho_c \Sigma_j (r_j^s \vartheta_{ji}^s)) \qquad i=N_2, O_2, CO, CO_2, H_2O \tag{15}$$

Carbon and hydrogen molar balance:

$$\frac{\partial N_{iLF}^s}{\partial z} = A_{LF} \varepsilon_{cLF} \rho_c \Sigma_j (r_j^s \vartheta_{ji}^s) \qquad i=C, H \tag{16}$$

Energy balance:

$$\Sigma_i F_{iLF} C_{p_i} \frac{\partial T_{LF}}{\partial z} = -A_{LF}(\varepsilon_{gLF} \Sigma_j (r_j^g \Delta H_j^g) + \varepsilon_{cLF} \rho_c \Sigma_j (r_j^s \Delta H_j^s)) \qquad i=N_2, O_2, CO, CO_2, H_2O \tag{17}$$

Overall, the mass balances around the regenerator in order to calculate catalyst bed level and gas inventory are according to the equations below [28]:

Catalyst inventory:

$$\frac{\partial W_{cRG}}{\partial t} = F_{cLF} - F_{cRG} - F_{rcRG} \tag{18}$$

Catalyst bed level:

$$L_{RG} = \frac{W_{cRG}}{\rho_c \varepsilon_{cRG} A_{RG}} \tag{19}$$

Gas inventory:

$$\frac{\partial W_{gRG}}{\partial t} = F_{gLF} + F_{aRG} - F_{gRG} + \Sigma_i F_{cLF} Y_{iLF} - \Sigma_i (F_{cRG} + F_{rcRG}) Y_{iRG} \qquad i=C, H \tag{20}$$

The regenerator section consists of two regions, the dense phase, where the catalysts, after passing through the lift section, separate from gases and collapse and form a dense bed, and the freeboard, where only the reaction between CO and CO_2 occurs in absence of catalysts.

Dense bed:

This region was modeled as a CSTR reactor. The mass and energy balances for this phase are studied according to the following equations [28]:

Molar balance for gaseous species:

$$V_{bed} \frac{\partial C_{iRG}}{\partial t} = N_{iLF}^g + N_{iRG}^a - N_{iRG}^g + V_{bed}\left(\varepsilon_{gRG} \sum_j (r_j^g \vartheta_{ji}^g) + \varepsilon_{cRG} \rho_c \sum_j (r_j^s \vartheta_{ji}^s)\right) \tag{21}$$

Carbon and hydrogen molar balance:

$$\frac{W_{cRG}}{Mw_i}\frac{\partial Y_{iRG}}{\partial t}=\frac{F_{cLF}}{Mw_i}-\frac{(F_{cRG}+F_{rcRG})}{Mw_i}X_{iRG}+V_{bed}\varepsilon_{cRG}\rho_c\Sigma_j(r_j^s\vartheta_{ji}^s) \quad i=C, H \tag{22}$$

Energy balance:

$$\frac{\partial(W_{cRG}C_{p_c}T_{RG}+W_{gRG}C_{p_g}T_{RG})}{\partial t}=F_{gLF}H_{gLF}+F_{cLF}H_{cLF}+Y_{ckLF}F_{cLF}H_{ckLF}+F_{aRG}H_{aRG}-Y_{ckRG}(F_{cRG}+F_{rcRG})H_{ckRG}$$

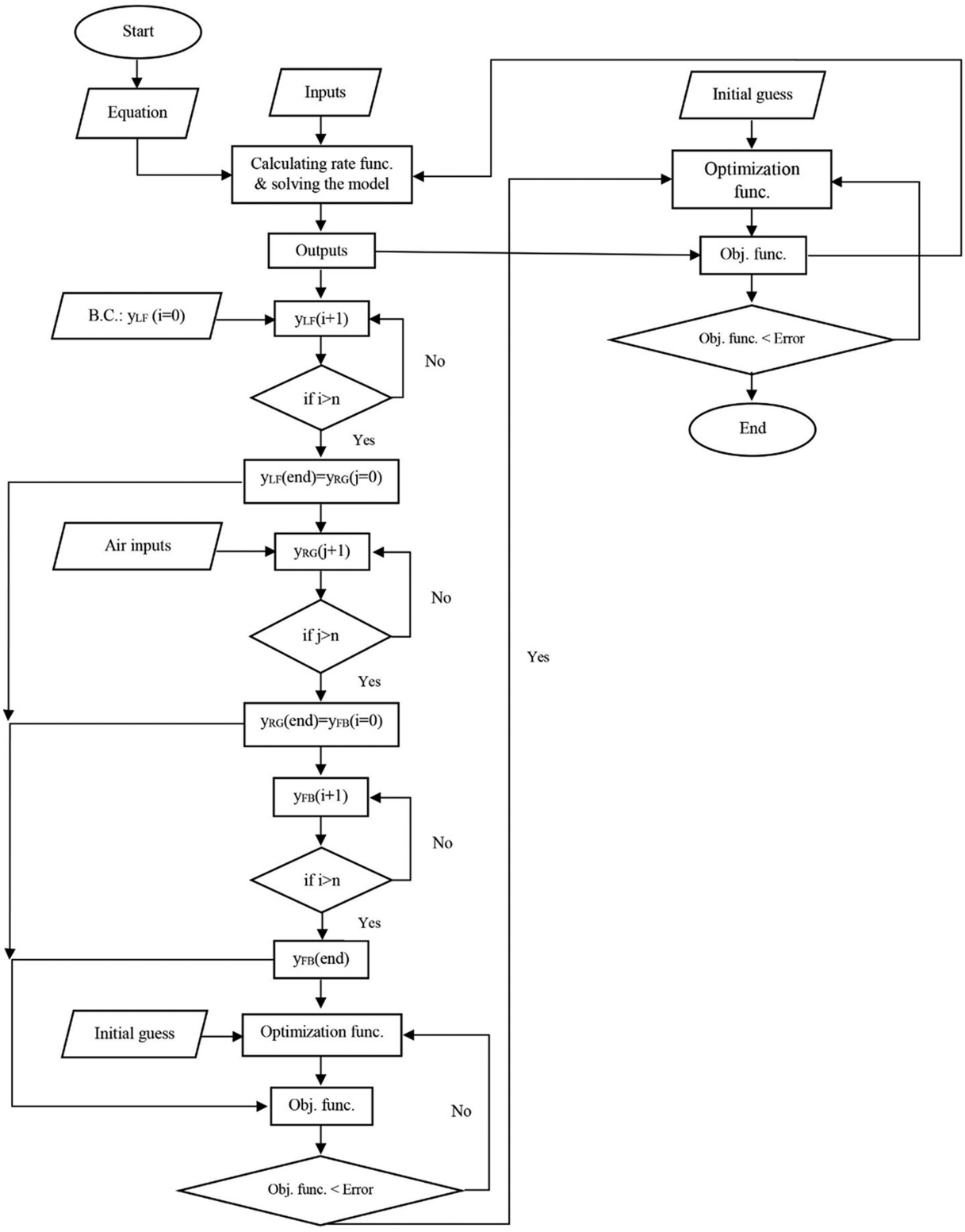

Fig. 4. The algorithm for solving the model and optimization.

$$-F_{gRG}H_{gRG}-(F_{cRG}+F_{rcRG})H_{cRG}+Q_r^0+Q_{loss} \quad (23)$$

Freeboard:

Molar balances for gaseous species:

$$\frac{\partial N_{iFB}^g}{\partial z}=A_{FB}\Sigma_j(r_j^g\vartheta_{ji}^g) \qquad i=N_2, O_2, CO, CO_2, H_2O \quad (24)$$

Energy balance:

$$\Sigma_i F_{iFB}C_{p_i}\frac{\partial T_{FB}}{\partial z}=-A_{FB}\Sigma_j(r_j^g\vartheta_{ji}^g)+\pi D_{FB}U_{FB}(T_{surr}-T_{FB})$$
$$i=N_2, O_2, CO, CO_2, H_2O \quad (25)$$

METHOD OF SOLVING AND OPTIMIZATION

Fig. 4 illustrates the algorithm for solving the model and optimization. The riser reactor model was solved using the PDEPE toolbox of MATLAB version R2016a (9.0.0.341360) which solves PDE equations based on the finite element method with high speed and accuracy, and the regenerator model was also solved following the discretization via Euler method. Evidently, the developed algorithm solves the modeling problem in three steps: the modeling of the riser, solving the regenerator governing equations and optimization.

After solving the model, kinetic constants were estimated with the aim of achieving more precise and consistent responses to the unit data using the objective function presented in Eq. (26), in which x_i is the mass fraction of each component. Finally, the outputs of the regenerator and the riser sections were utilized for unit optimization using the Levenberg-Marquardt algorithm, which solves nonlinear least square problems. Nonlinear least squares methods iteratively reduce the sum of the squares of the errors between the function and the observed parameters through a sequence of updates of the parameter values [48]. In this way, the objective function is considered in order to model two forms, i.e., one maximizing the yield of production gasoline and the other maximizing the yield of gasoline and the RON, both of which perform due to the existing conditions according to the following equations. The appropriate inequality constraints, which are defined according to the industrial plant operating data, are presented in Eqs. (29) to (32). Other optimization goals included increasing the unit profitability and reducing the energy consumption.

$$f(x)=\sum_{i=1}^{n}\left(\frac{x_i^{model}-x_i^{plant}}{x_i^{plant}}\right)^2 \quad (26)$$

$$f(x)=\sum_{i=1}^{n}\left(\frac{x_{Gasoline}^{model}-x_{Gasoline}^{max}}{x_{Gasoline}^{max}}\right)^2 \quad (27)$$

$$f(x)=\sum_{i=1}^{n}\left(\frac{x_{Gasoline}^{model}-x_{Gasoline}^{max}}{x_{Gasoline}^{max}}\right)^2+\left(\frac{RON^{model}-RON^{max}}{RON^{max}}\right)^2 \quad (28)$$

$$F_{tf}^l\le F_{tf}\le F_{tf}^u \quad (29)$$

$$F_{cRG}^l\le F_{cRG}\le F_{cRG}^u \quad (30)$$

$$F_c^l\le F_c\le F_c^u \quad (31)$$

$$T_{tf}^l\le T_{tf}\le T_{tf}^u \quad (32)$$

Table 1. The Abadan refinery FCC unit dimensions

FCC unit dimensions	Length (m)	Diameter (m)
Riser	25	1.17
Combustor	12.75	6.7
Lift section	13	3
Regenerator	21	9.4

Table 2. Catalyst heat capacity and flow rates

Parameter	Value
Spent catalyst flow rate (kg/s)	466.67
Regenerated catalyst flow rate (kg/s)	464.1
Heat capacity j/(kg K)	1,197.5

where l and u are the lower and upper limits of each parameter, which were considered ±2% of the average of each parameter of the Abadan refinery high-efficiency FCC unit (industrial plants operate in a certain operating conditions range, and any changes must be around the same range). In this case, the values are: total feed flow rate (70-74 kg/s), the regenerated catalyst flow rate (457-476 kg/s), spent catalyst flow rate (460-480 kg/s) and feed preheat temperature (483-500 K).

The Abadan refinery high-efficiency FCC dimensions are presented in Table 1. Heat capacity and flow rates of catalyst are also presented in Table 2.

RESULTS AND DISCUSSION

The values of the parameters used to solve the model in the dynamic mode are given in Tables 3 and 4. Our data are industrial data and were gathered from the Abadan refinery FCC unit over ten days at the time of unit stability, so the data can be assumed to be reproducible and the limited deviations are due to accidental and uncontrollable sources of error. These values include reactor and regenerator pressure, regenerator and combustor temperature, the rate of inlet air flow to the regenerator, feed flow rate and feed density. As shown in the table below, the feed flow enters the riser at an average flow rate of 72.22 kg/s and an average temperature of 492.85 K. Meanwhile, the inlet air moves toward the combustor at a flow rate of approximately 61.2 kg/s. The average output temperature of the unit reactor is 793.25 K and the regenerator temperature is within the range of 1,011.15 K to 1,017.15 K, while the combustor temperature ranges from 949.15 K to 956.25 K. The regenerator pressure was fixed at 1.8 bar and the riser reactor pressure fluctuated between 1.322 and 1.333 bar.

In addition, the industry data on product yields (LCO, gasoline, LPG, dry gas and coke) taken over ten days are given in Table 4. Data from the target refinery reveals that gasoline is the main product of the unit, with an average flow rate of about 32.1 kg/s.

The catalyst applied in the selected FCC unit is zeolite with a 0.87 SiO_2/Al_2O_3 ratio. The catalyst physical properties are presented in Table 5. Al_2O_3 and SiO_2 comprise the largest share (approximately 51% and 44%, respectively) of the total catalyst and the rest are made up of components, such as Fe, V, Ni and CaO. The aver-

Table 3. Industrial data of the Abadan refinery FCC unit

Day	Feed (kg/s)	Reactor pressure (bar)	Main air blower (kg/s)	Fluffing air (kg/s)	Fluffing air (kg/s)	Regen. temp. (K)	Combustor temp. (K)	Regen. press. (bar)	Raw oil preheat temp. (K)	Reactor to main column temp. (K)	Feed Sp. Gr.
1	72.18	1.322	61.25	0.63	0.65	1,011.15	949.95	1.8	493.35	793.15	0.909
2	72.15	1.332	61.33	0.61	0.64	1,014.15	954.85	1.8	494.55	793.15	0.91
3	72.11	1.323	61.24	0.61	0.64	1,013.15	954.55	1.8	495.25	793.15	0.911
4	71.93	1.331	61.2	0.61	0.65	1,013.15	951.35	1.8	495.15	793.15	0.911
5	71.87	1.323	61.31	0.62	0.65	1,017.15	956.25	1.8	492.25	793.15	0.911
6	72.05	1.321	61.31	0.62	0.65	1,016.15	956.25	1.8	492.65	793.15	0.914
7	72.17	1.326	61.16	0.61	0.65	1,015.15	954.25	1.8	492.55	793.15	0.913
8	72.39	1.333	61.06	0.61	0.65	1,014.15	949.15	1.8	491.25	793.15	0.905
9	72.22	1.333	61	0.61	0.65	1,014.15	948.05	1.8	490.65	793.15	0.913
10	72.47	1.332	61.07	0.62	0.65	1,012.15	949.85	1.8	490.85	794.15	0.91

Table 4. Industrial data of the Abadan refinery FCC unit products

Day	LCO		Gasoline		LPG		Dry gas		Coke	
	Flow rate (kg/s)	Mass frac.	Flow rate (kg/s)	Mass frac.	Flow rate (kg/s)	Mass frac.	Flow rate (kg/s)	Mass frac.	Flow rate (kg/s)	Mass frac.
1	13.91	0.193	32.16	0.446	10.37	0.144	3.01	0.042	5.88	0.081
2	13.81	0.191	31.91	0.442	10.48	0.145	3.06	0.042	5.9	0.082
3	14.24	0.197	31.84	0.442	10.49	0.145	3.09	0.043	5.97	0.087
4	13.63	0.189	32.18	0.447	10.2	0.142	3.02	0.042	5.99	0.083
5	13.7	0.191	31.83	0.443	10.16	0.141	3.13	0.043	5.99	0.083
6	13.88	0.193	31.98	0.444	10	0.139	3.16	0.044	6.17	0.086
7	13.72	0.190	32.09	0.445	10.2	0.141	3.19	0.044	5.95	0.083
8	13.88	0.192	32.21	0.445	10.15	0.140	3.15	0.044	6.17	0.085
9	13.94	0.193	32.4	0.449	10.14	0.140	3.21	0.045	5.9	0.082
10	13.73	0.189	32.42	0.447	10.18	0.140	3.24	0.045	6.44	0.089

Table 5. The catalyst physical properties of the Abadan refinery FCC unit

Parameter	Value
Al_2O_3 (wt%)	51.1
SiO_2 (wt%)	44.5
Total surface area (SA) (m^2/g)	149
Pore volume (cm^3/g)	0.43
Particle density (kg/m^3)	1,220
Average particle size (APS) (μm)	84

Table 6. The kinetic constants related to the cracking reactions occurring in the riser

Reactions	Pre-exponential factor	Activation energy (J/mol)
VGO→LCO	9.31×10^5 ($m^3/s/kg$)	84.2×10^3
VGO→GLN	3.5×10^5 ($m^3/s/kg$)	84.2×10^3
VGO→LPG	2.57×10^5 ($m^3/s/kg$)	84.2×10^3
VGO→FG	4.13×10^4 ($m^3/s/kg$)	84.2×10^3
VGO→CK	4.99×10^5 ($m^3/s/kg$)	84.02×10^3
LCO→GLN	2.9×10^4 (s^{-1})	77.1×10^3
LCO→CK	6.13×10^3 (s^{-1})	77.1×10^3
GLN→LPG	3.91×10^8 (s^{-1})	146×10^3
GLN→FG	1.26×10^8 (s^{-1})	146×10^3
LPG→FG	1.05×10^{11} (s^{-1})	193×10^3

age catalyst density, the average particle size of the catalyst, total surface area and pore volume, are about 1,220 kg/m^3, 84 μm, 149 m^2/g and 0.43 cm^3/g, respectively.

1. Kinetic Parameter Estimations

The estimation of kinetic constants is an influential yet difficult part of model improvement. Therefore, the error between model results and industry data was minimized in order to achieve more accuracy and compatibility with industrial data. To achieve this, optimization was carried out. The initial estimates of rate constants were generated based on the data gathered from literature review of research on FCC units with the closest condition to the target plant [28,44]. Then the Levenberg-Marquart optimization algorithm was applied as an effective method to solve the proposed optimization objective function to minimize the error between the model and the collected industrial data.

The kinetic constants estimated in relation to the cracking reactions occurring in the riser and the reactions occurring in the regenerator are represented in Tables 6 and 7, respectively. Since the

Table 7. Kinetic constant related to the reactions occurring in the regenerator

Kinetic parameter	Value
k_{C1}^{dry}	1.18×10^{3}
k_{C1}^{wet}	4.31×10^{4}
k_{C2}^{dry}	7.84×10^{1}
k_{C2}^{wet}	2.53×10^{5}
k_{C3}^{wet}	1.31×10^{3}
k_{3}^{s}	4.03×10^{1}
k_{4}^{s}	3.89×10^{-12}
k_{1}^{g}	8.45×10^{19}
E_{C1}^{dry}	1.43×10^{5}
E_{C1}^{wet}	7.92×10^{4}
E_{C2}^{dry}	0.159×10^{1}
E_{C2}^{wet}	1.75×10^{4}
E_{C3}^{wet}	2.71×10^{4}
E_{a3}^{s}	2.69×10^{5}
E_{a4}^{s}	1.15×10^{4}
E_{a1}^{g}	2.63×10^{5}

industrial data were used to determine the coefficients of rate constants and to validate, the kinetic model is suitable to be applied on FCC plants which are designed based on the high-efficiency technology with operating conditions including pressure, temperature, and flow rates.

2. Dynamic Model Results

Fig. 5 shows the model results of the unit, which includes the mass fraction of the products. It is also clear in the figure that gasoline is the main product of the unit. The zero time (0 sec) in the figures is the start time of the dynamic phenomena and it is not related to the start-up time of the process or riser-reactor.

The values of parameters, such as heat capacity, enthalpy and physical properties—including density and molecular weight of each feed component—have a significant effect on unit performance due to their variation over time and their dependence on various operating conditions, namely temperature and pressure. Herein, all of the aforementioned parameters and several others, such as the height and volume of the fluidized bed and the volume fraction of the gas and catalyst, were considered as the variables of the operating conditions and time, thus augmenting the accuracy of the results.

In addition to the parameters mentioned above, residence time was considered as a function of the input feed flow rate. It was observed that the residence time variations were between 2.8 and 3.3 s. In the section on dynamic analysis and unit optimization, it was mentioned that changes in feed flow rate change the residence time of the riser reactor. Therefore, considering this parameter variable increased the accuracy of the obtained results.

Table 8. Model validation results

Output	MRE	RMSE
LCO	0.0162	0.0036
Gasoline	0.0038	0.0021
LPG	0.0276	0.0041
Dry gas	0.0255	0.0013
Coke	0.0370	0.0034
Temperature	0.0028	0.0239

3. Results Validation

The validation was performed using mean relative error (MRE), and root mean square error (RMSE) was calculated through implementing the model results and the plant outputs. As observed in Table 8, the validation results reveal the high accuracy of the model. The MRE and RMSE for gasoline as the main product are 0.0038 and 0.0021, respectively. It is indicated that the model outputs are accurate and consistent with the output data of the selected FCC unit.

Fig. 6 depicts the graph indicating the trend of the model results in comparison with the plant data for each component. The results are evidently in the same range and also have the same trend as the

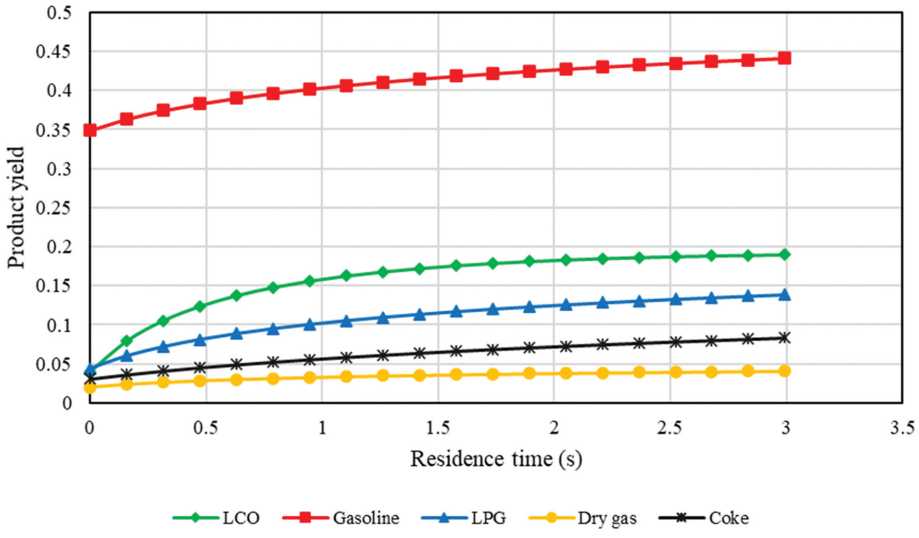

Fig. 5. Results of dynamic model for the Abadan refinery FCC unit.

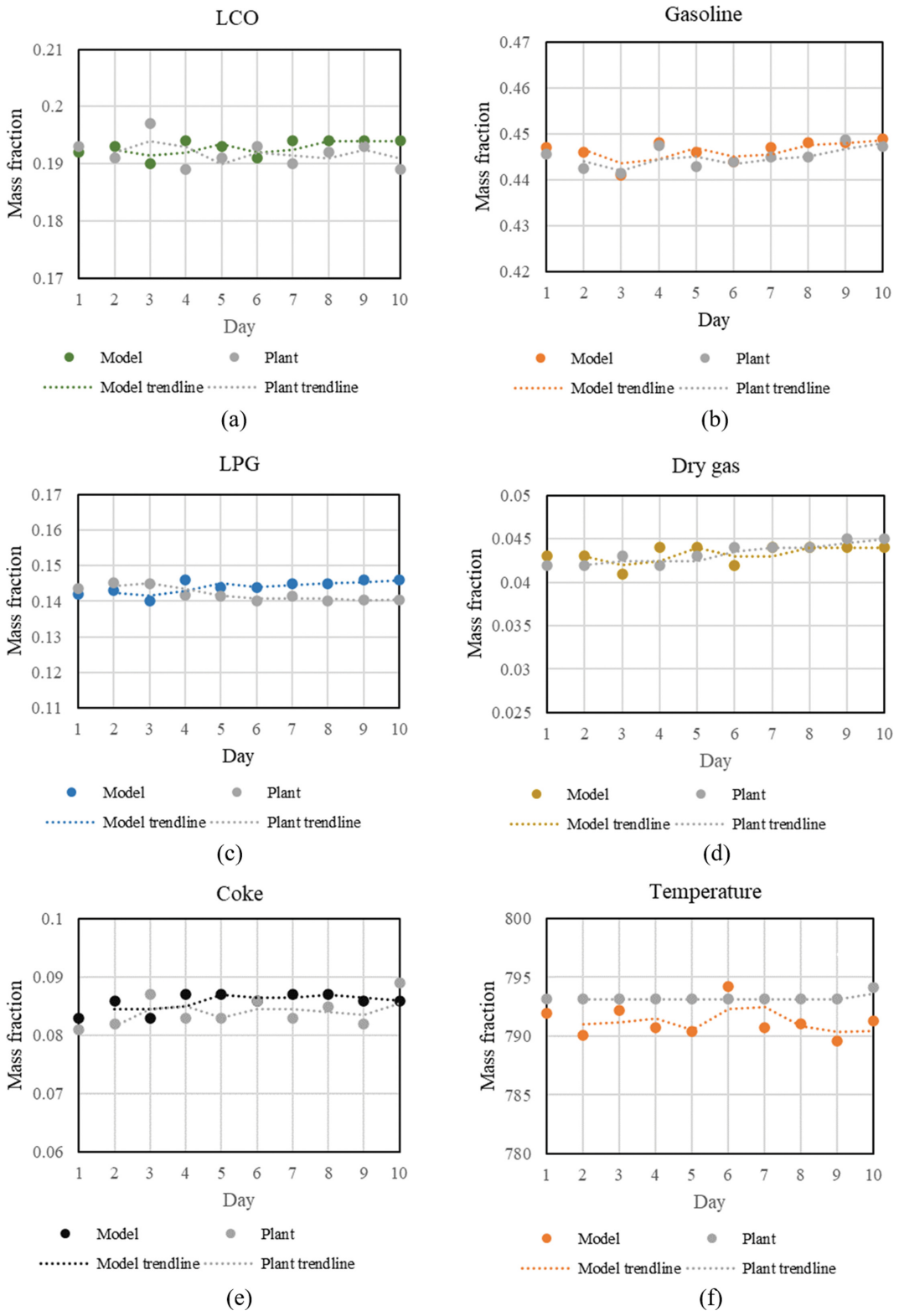

Fig. 6. Model validation with plant data: (a) LCO, (b) Gasoline, (c) LPG, (d) Dry gas, (e) Coke, (f) Temperature.

plant data.

4. Operating Conditions Effect Analysis

Turbulence in operating conditions is an integral part of refinery units that impede unit performance and product yield. Therefore, it is necessary to identify and resolve negative effects by examining their influence on the unit performance. In this section, the effects of gradual and sudden changes in operating conditions on gasoline and LCO yields (as main products of the unit) and riser

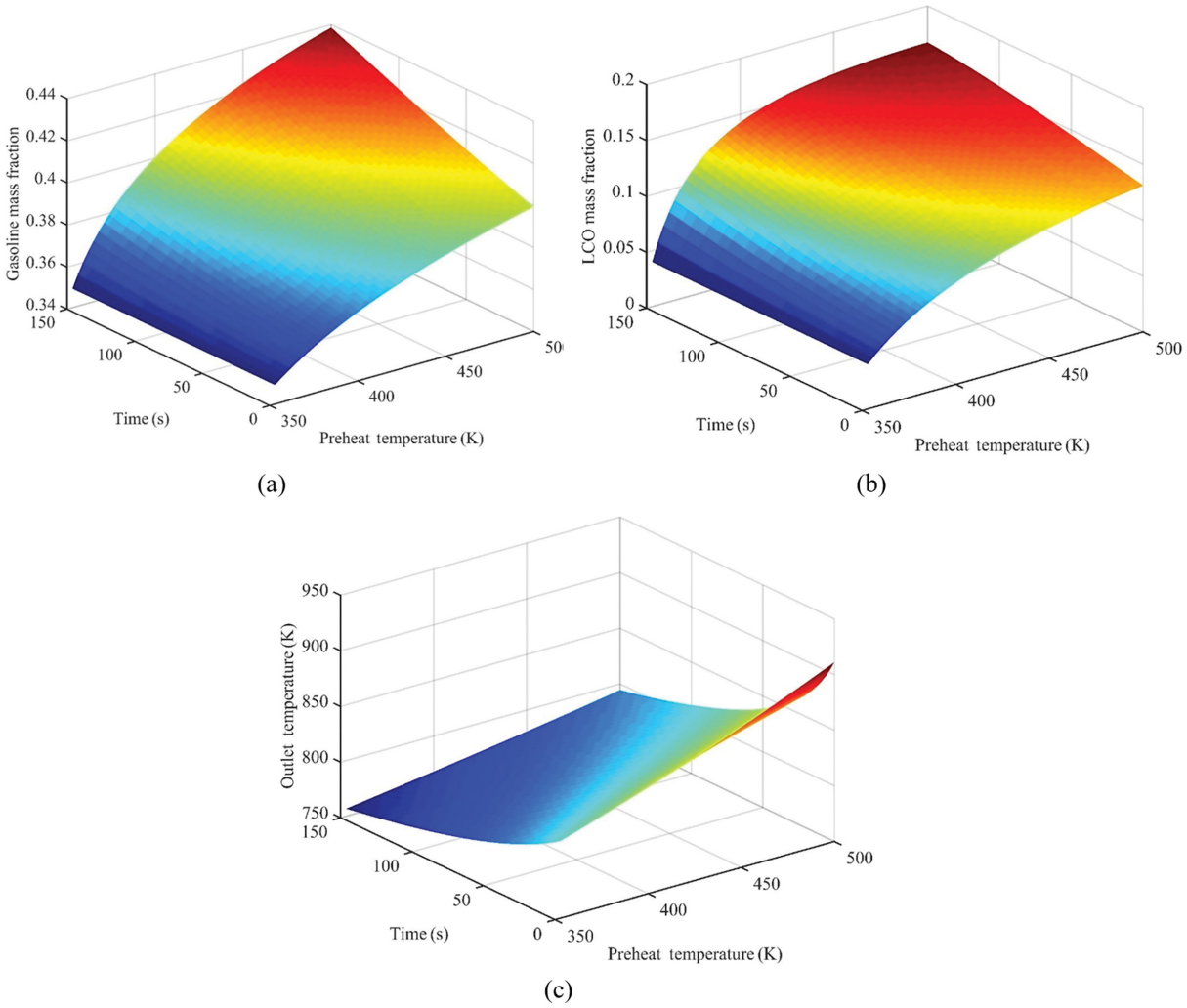

Fig. 7. The effect of increasing the feed preheat temperature on: (a) Gasoline mass fraction, (b) LCO mass fraction, (c) Outlet temperature.

outlet temperature were investigated.

4-1. Gradual Changes in Feed Preheat Temperature

Fig. 7(a) displays the effect of increasing the feed preheat temperature on the yield of gasoline. Since the cracking reactions are endothermic, they will be further increased with higher temperature. By increasing the feed preheat temperature and the time passing, the gasoline mass fraction increased to about 0.43, in which, in higher temperature, a steeper slope is observed due to the increasing rate of cracking reactions. Fig. 7(b) also shows the effect of increasing feed preheat temperature on the yield of LCO. Some reactions were performed more quickly with regard to the kinetic constants and, following this, some products, such as gasoline, will be produced more quickly, which will increase the amount of other products to a lesser extent and, after a while, the slope is reduced. Regarding the kinetic network shown in Fig. 3, it can be seen that LCO is the only product whose consumable reactions are more than its production reactions. As a result, by increasing temperature, which is accompanied by an increase in the speed of the reaction, its consumption rate will eventually increase with a slight slope.

As shown in Fig. 7(c), the riser output temperature increases by increasing feed preheat temperature and also decreases over time. The reason for the decrease in temperature over time is that, by increasing the feed preheat temperature, the cracking reactions, which are endothermic reactions, have occurred to a greater extent, and this is why more heat is taken from the system, which over time reduces the output temperature of the riser.

4-2. Sudden Changes in Operating Conditions

Fig. 8(a) shows that a sudden drop in the feed preheat temperature of 30 K causes the gasoline yield to decrease by about 2% due to the endothermic reactions occurring in the riser. Therefore, when the feed preheat temperature decreases, the reactions occur at a slower rate, thereby reducing the amount of gasoline produced. It was observed that the negative effect of this change was neutralized by a 4% increase in the regenerated catalyst flow rate and a 6% decrease in the feed flow rate, which caused the gasoline yield to return to its previous level (0.443). As it is known, refinery units operate in a certain operating conditions range, and any changes must be around the same range. To compensate for the negative effect of sudden variation, improved operating conditions were determined using trial and error in the permitted operating range. To apply these changes, the dynamic model was run over a speci-

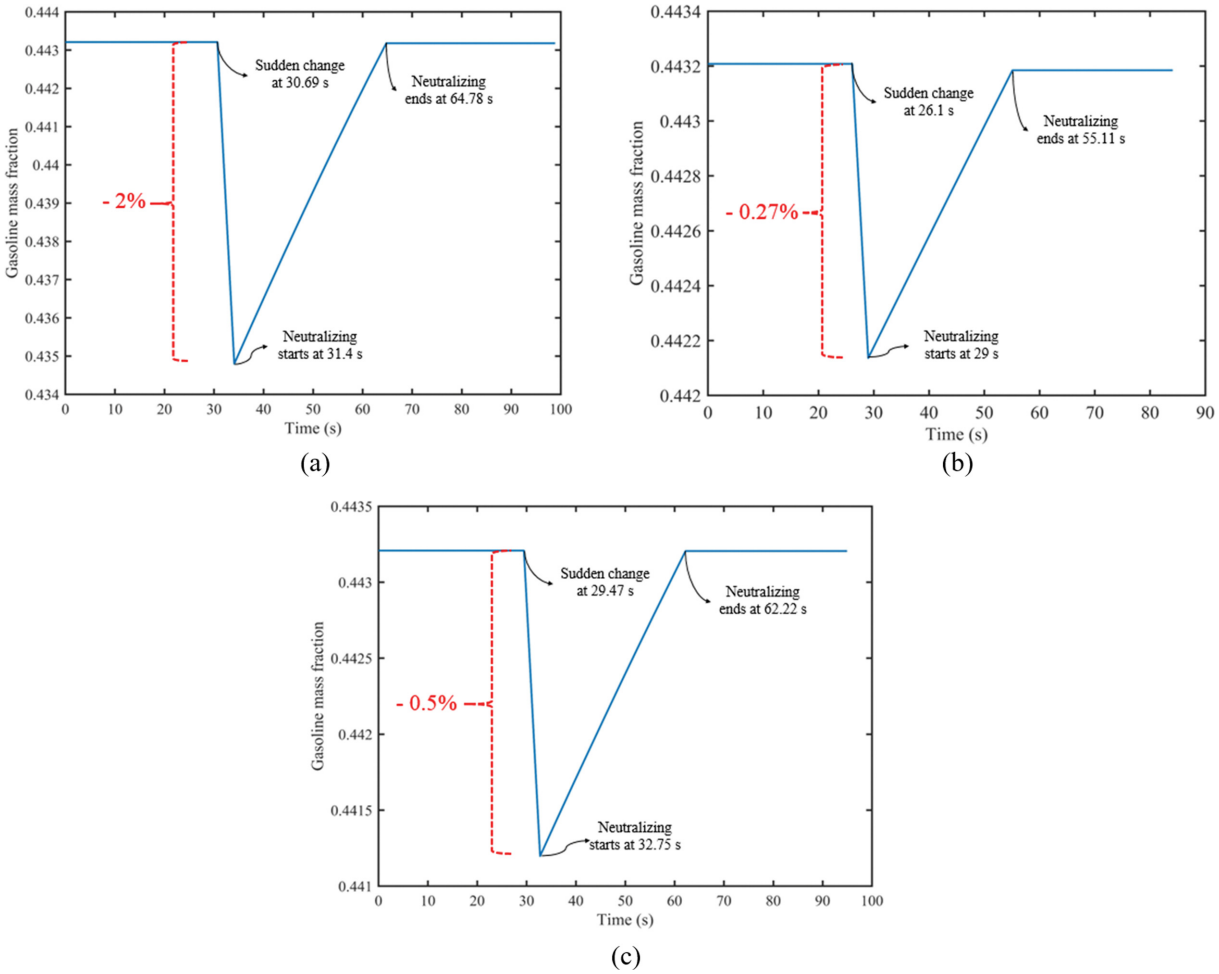

Fig. 8. The effect of different parameters change on gasoline yield and its neutralization: (a) Feed preheat temperature, (b) Feed flow rate, (c) Regenerated catalyst flow rate.

fied time interval divided into 30 steps; each step was equivalent to the reactor residence time. Afterward, at each step, the feed flow rate was reduced by 0.6 kg/s, and 1.76 kg/s was added to the regenerated catalyst flow rate. Applying these changes for 30.68 s brought the gasoline yield back to the previous value. These values were obtained by the model for the target unit and might be different in the other FCC units due to the control system and instrumentation equipment used, which vary according to different operating conditions.

As shown in Fig. 8(b), gasoline yields decreased by 0.27% when the feed flow rate was suddenly increased by 6.9%. The reason is that, after increasing the feed flow rate, the same amount of previous catalyst flow rate is insufficient for instigating the reactions. As a result, reactions occur less frequently and the yield of gasoline is reduced. To neutralize the negative effect of this change, a 0.83% increase in the regenerated catalyst flow rate and a 1.5 K decrease in feed preheat temperature enabled the gasoline yield to reach its previous level after 26.11 seconds. To make these changes, the catalyst flow rate was increased by 0.37 kg/s and the feed preheat temperature was reduced by 0.15 K at each time step.

Fig. 8(c) shows that a sudden drop in the regenerated catalyst flow rate of 1.12% caused the gasoline yield to decrease by 0.5%. Furthermore, a reduction in the regenerated catalyst flow rate with no change in the feed flow rate led to an insufficient catalyst level for converting feed into products. In this case, the reaction occurring in the riser is slower and, as a result, less gasoline is produced. It was observed that a 5.5% decrease in the feed flow rate and a 5 K increase in the feed preheat temperature enabled the gasoline yield to return to its previous level after 29.47 seconds. To make these changes, the feed flow was reduced by 0.38 kg/s and the feed preheat temperature was increased by 0.5 K at each time step.

As a result, the effect of feed preheat temperature sudden change on the gasoline yield was by far greater than the effects of feed and catalyst flow rates sudden change, so that the amount of gasoline yield reduction because of sudden temperature drop was 4 and 7 times higher than that of feed and catalyst flow rate, respectively. At a first glance, this change in the yield of produced gasoline may not seem significant. However, these seemingly minor changes, if not resolved, would cause losses of approximately $1.5 to $12 million per year.

5. Optimization

In this section, the optimization results aimed at increasing the gasoline yield, reduce energy consumption and improve the RON are presented. Parameters involved in optimization include feed,

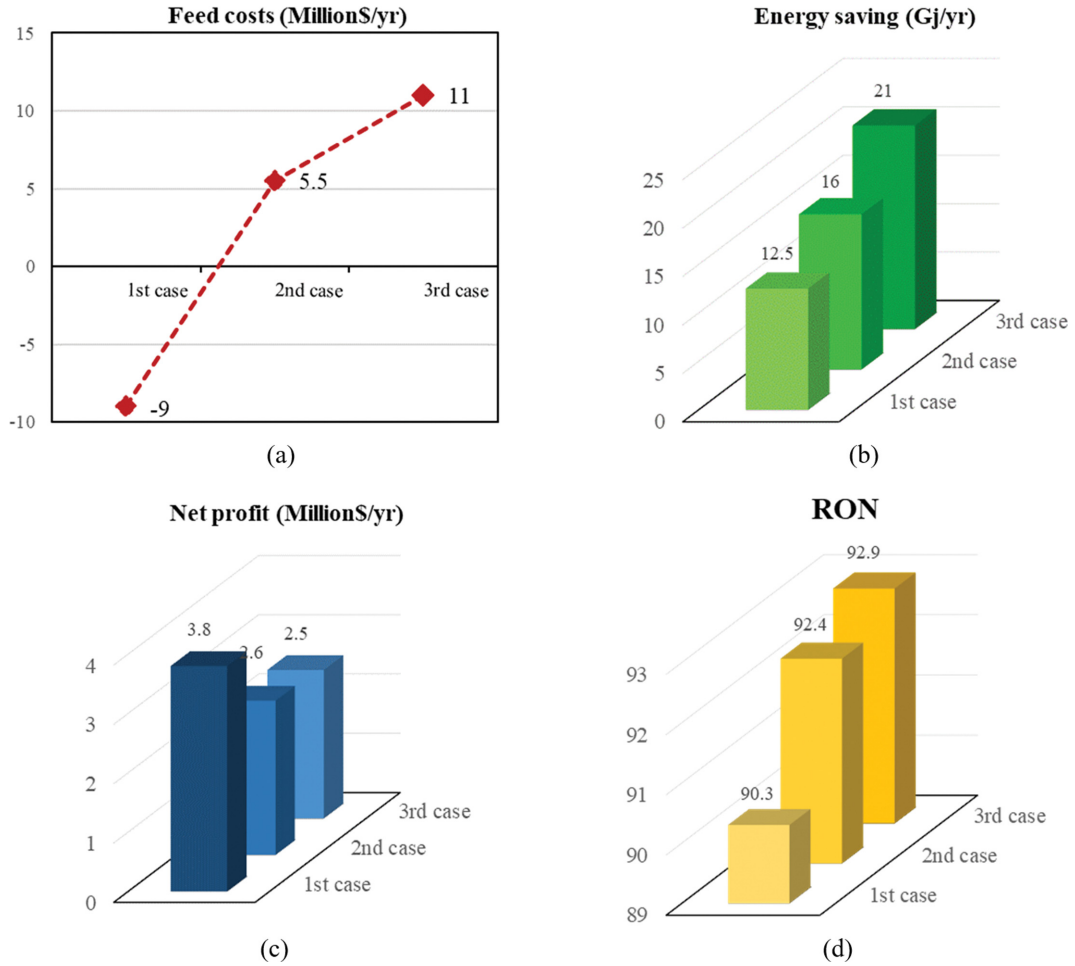

Fig. 9. Optimization results for each case: (a) Feed costs, (b) Energy saving, (c) Net profit, (d) RON.

Table 9. Optimal values for each of the optimization parameters

State \ Parameter	Feed (kg/s)		Catalyst flow rate (kg/s)		Inlet temperature (K)		RON		Profitability (Million$/yr)
	Actual	Optimal	Actual	Optimal	Actual	Optimal	Actual	Optimal	Optimal
First state	72.174	71.117	466.7	462.7	492.98	488.53	92.3	92.3	3.8
Second state	72.174	72.922	466.7	465.63	492.98	487.41	92.3	92.4	2.6
Third state	72.174	73.644	466.7	471.99	492.98	485.78	92.3	92.9	2.5

catalyst flow rate and feed internal temperature. The optimization was performed with three approaches: unrestricted to octane number, maintaining the average octane number and improving the octane number. Fig. 9 exhibits the optimization results presented in three cases: the amount of feed cost (Fig. 9(a)), energy-saving (Fig. 9(b)), unit profitability (Fig. 9(c)) and octane number (Fig. 9(d)) for each case.

In the first case, with the objective of increasing the gasoline yield while remaining unrestricted to octane number, the reduction of feed, catalyst flow rate and inlet temperature caused an increase in the yield of the gasoline by 0.67% and the octane number reached 92.3, which is equal to the unit average. The results implied a nearly $9 million reduction in feed costs per year, a 12,500 Gj reduction in energy consumption and, subsequently, a profit of $3.8 million per year, which is about 44% higher than the unit average.

In case two, aimed at increasing the gasoline yield and maintaining the average octane number, the increased feed, the reduction of catalyst and the inlet temperature caused a rise in the yield of the gasoline by 0.45% and the octane number was maintained at 92.4. The results showed an increase in feed costs by about $5.5 million per year, a reduction of 16,000 Gj in energy consumption and, lastly, a profit of $2.6 million per year, which is about 30.6% higher than the unit average.

Finally, in the third case, considering the increasing in the gasoline yield and improving the octane number, increased feed, catalyst, and reduced inlet temperature caused an increase of the yield

of the gasoline by 0.45% and the octane number reached 92.9, which is greater than the unit average and the maximum possible. The results show that, in this case, feed costs would increase by about $11 million per year, as well as a 21,000 Gj reduction in energy consumption and, finally, a profit of $2.5 million per year, which is about 28.8% higher than the unit average. Table 9 also shows the optimal values for each of the optimization parameters in summary.

The profitability resulted from just increasing the gasoline yield and change of the feed and catalyst flow rates of the unit has been calculated for each three optimization cases, using the data received from the Abadan refinery FCC unit and also the price of FOB Persian Gulf gasoline.

CONCLUSION

The fluidized catalytic cracking unit of the Abadan Refinery was optimized. Kinetic constants were estimated and the effects of changes in feed preheat temperature on the unit main products were investigated. The results are in good agreement with the industrial data. According to which, in addition to increasing gasoline yield and improving the octane number, reductions in catalyst flow rate in the range of one to four kg/s and an energy consumption in the range of 12.5-21 Gj/yr were achieved. By gradually increasing the feed preheat temperature, the gasoline mass fraction was increased to about 0.44 and the yield of LCO was increased to about 0.17. The results also reveal that the most effective parameter on gasoline yield is the regenerated catalyst flow rate.

Based on the optimization results, feed costs would be reduced by about $9 million per year, increased by about $5.5 million per year and increased by about $11 million annually in the first, second and third cases, respectively. The reductions in energy consumption would be about 12,500, 16,000 and 21,000 Gj for the first, second and third cases, respectively. The first, second and third cases are associated with the profits of $3.8 million, $2.6 million and $2.5 million per year, respectively. These profits represent increases of about 44%, 30.6% and 28.8% when compared with the average for the first, second and third cases, respectively.

Generally, the first and the third cases are better than the second one. The first case has the highest profitability and the highest gasoline yield; on the other hand, the third case has the highest octane number and the greatest energy reduction.

Future research will be carried out through multivariate optimization approach to consider all variables interactions, obtaining the most efficient operational conditions of the unit such as studies carried out based on multivariate method [49,50].

ACKNOWLEDGEMENT

The financial support provided by the Research and Development of Abadan refinery complex is greatly appreciated.

NOMENCLATURE

A : cross-sectional area [m]
A_{ij} : pre-exponential factor of the reaction lump i→lump j [m^3/(s kg) or s^{-1}]
C_i : molar concentration of lump i [mol/m^3]
$\hat{C}_i$: mass concentration of lump i [kg/m^3]
C_P : specific heat capacity [j/kg K]
D : diameter [m]
E_{ij} : activation energy of the reaction lump i lump j [J/mol]
E_C : energy parameter of the carbon combustion reaction [J/mol]
E^s_{aj} : activation energy of the gas-solid reaction [J/mol]
E^g_{aj} : activation energy of the gas reaction [J/mol]
F : mass flow rate [kg/s]
FG : flue gas
G_c : solid mass flux [kg/m^2 s]
GLN : gasoline
g : gravity acceleration [m/s^2]
H : enthalpy [m/s^2]
k_C : rate coefficient of the carbon combustion reaction
k^g_j : kinetic rate constant of the gas reaction j [mol s^{-1} m^{-3}]
k^s_j : kinetic rate constant of the gas-solid reaction j [mol s^{-1} kg^{-1} cat]
L : height [m]
LCO : light cycle oil
LPG : liquefied petroleum gas
Mw : molecular weight [kg/mol]
MRE : mean relative error
N : molar flow rate [mol/s]
n_{ij} : order of the reaction lump i→lump j
P : pressure [Pa]
Q_{loss} : heat loss [J/s]
Q^0_r : Global reaction heat at standard conditions [J/s]
R : Universal gas constant [J/mol K]
r_C : intrinsic carbon combustion rate [mol (kg catalyst)$^{-1}$ s^{-1}]
r_{ij} : rate of reaction lump i→lump j [kg/m^3 s]
r_i : rate of formation of i [kg/m^3 s]
r^g_j : rate of gas reaction j [mol/m^3 s]
r^s_j : rate of gas-solid reaction j [mol/kg s]
RMSE : root mean square error
Sp. Gr. : specific gravity
T : temperature [K]
t : time [s]
u : superficial velocity [m/s]
U : overall heat transfer coefficient [J/m^2 s K]
V : volume [m^3]
W : inventory [kg]
x_i : mass fraction of i
Y^{cat}_{ck} : catalytic coke content of catalyst [kg coke/kg catalyst]
y_i : molar fraction of i
Y_i : component i (in coke) content of catalyst
z : axial coordinate[m]
ΔH : heat of reaction [J/kg]
ΔH_{crk} : heat of cracking per unit mass of VGO [J/kg]
α_c : deactivation constant [kg catalyst/kg catalytic coke]
σ : intrinsic CO_2/CO molar ratio in coke [dimensionless]
ε : volume fraction [dimensionless]
φ : catalyst deactivation function [dimensionless]
ρ : density [kg/m^3]
ϑ^s_{ji} : stoichiometric coefficient of lump i in gas-solid reaction j

[dimensionless]

ϑ_{ji}^{g} : stoichiometric coefficient of lump i in gas reaction j [dimensionless]

Subscripts

a : air
c : catalyst
ck : coke
FB : freeboard section
g : gas
LF : lift section
m : mean
ov : feed vapor
rc : recirculated catalyst
RG : regenerator section
rs : riser
surr : surrounding
tf : total feed
VGO : vacuum gas oil
1 : refers to the lift and the combustor section
2 : refers to the dense bed and freeboard

REFERENCES

1. R. Sadeghbeigi, *Fluid catalytic cracking handbook*, Elsevier (1995).
2. V. W. Weekman Jr. and D. M. Nace, *AIChE J.*, **16**, 397 (1970).
3. L. S. Lee, Y. W. Chen, T. N. Huang and W. Y. Pan, *Can. J. Chem. Eng.*, **67**, 615 (1989).
4. J. Ancheyta-Juárez, F. López-Isunza, E. Aguilar-Rodríguez and J. C. Moreno-Mayorga, *Ind. Eng. Chem. Res.*, **36**, 5170 (1997).
5. M. Fabulic Ruszkowski, Z. Gomzi and T. Tomic, *Chem. Biochem. Eng. Q.*, **20**, 61 (2006).
6. G. Bollas, A. Lappas, D. Iatridis and I. Vasalos, *Catal. Today*, **127**, 31 (2007).
7. J. Ancheyta-Juárez and J. A. Murillo-Hernández, *Energy Fuels*, **14**, 373 (2000).
8. L. Yen, R. Wrench and A. Ong, *Oil Gas J.; (United States)*, **86** (1988).
9. J. Ancheyta-Juarez and R. Sotelo-Boyas, *Energy Fuels*, **14**, 1226 (2000).
10. K. Sertić-Bionda, Z. Gomzi and M. Mužic, *Chem. Eng. Commun.*, **197**, 275 (2009).
11. A. Blasetti and H. de Lasa, *Ind. Eng. Chem. Res.*, **36**, 3223 (1997).
12. H. Farag, A. Blasetti and H. de Lasa, *Ind. Eng. Chem. Res.*, **33**, 3131 (1994).
13. I. Pitault, M. Forissier and J. R. Bernard, *Can. J. Chem. Eng.*, **73**, 498 (1995).
14. S. Sadighi, A. Ahmad and M. Rashidzadeh, *Korean J. Chem. Eng.*, **27**, 1099 (2010).
15. Y. M. John, M. A. Mustafa, R. Patel and I. M. Mujtaba, *Fuel*, **235**, 1436 (2019).
16. A. G. Sani, H. A. Ebrahim and M. Azarhoosh, *Fuel*, **225**, 322 (2018).
17. H. Ali and S. Rohani, *Chem. Eng. Technol.: Ind. Chem.-Plant Equipment-Process Eng.-Biotechnol.*, **20**, 118 (1997).
18. A. Arbel, Z. Huang, I. H. Rinard, R. Shinnar and A. V. Sapre, *Ind. Eng. Chem. Res.*, **34**, 1228 (1995).
19. S. M. Jacob, B. Gross, S. E. Voltz and V. W. Weekman Jr., *AIChE J.*, **22**, 701 (1976).
20. A. Secchi, M. Santos, G. Neumann and J. Trierweiler, *Comput. Chem. Eng.*, **25**, 851 (2001).
21. S. Kim, J. Urm, D. S. Kim, K. Lee and J. M. Lee, *Korean J. Chem. Eng.*, **35**, 2327 (2018).
22. I.-S. Han and C.-B. Chung, *Chem. Eng. Sci.*, **56**, 1951 (2001).
23. Y. M. John, R. Patel and I. M. Mujtaba, *Comput. Chem. Eng.*, **106**, 730 (2017).
24. T. Takatsuka, S. Sato, Y. Morimoto and H. Hashimoto, *Int. Chem. Eng.*, **27**, 107 (1987).
25. J. Fernandes, J. J. Verstraete, C. C. Pinheiro, N. Oliveira and F. R. Ribeiro, *Comput. Aided Chem. Eng.*, **20**, 589 (2005).
26. J. L. Fernandes, C. I. Pinheiro, N. Oliveira and F. R. Ribeiro, *Comput. Aided Chem. Eng.*, **21**, 1575 (2006).
27. J. L. Fernandes, C. I. Pinheiro, N. M. Oliveira, A. I. Neto and F. R. Ribeiro, *Chem. Eng. Sci.*, **62**, 6308 (2007).
28. J. L. Fernandes, L. H. Domingues, C. I. Pinheiro, N. M. Oliveira and F. R. Ribeiro, *Fuel*, **97**, 97 (2012).
29. I.-S. Han, J. B. Riggs and C.-B. Chung, *Chem. Eng. Process.: Process Intensification*, **43**, 1063 (2004).
30. J. R. Hernández-Barajas, R. Vázquez-Román and D. Salazar-Sotelo, *Fuel*, **85**, 849 (2006).
31. R. B. Kasat, D. Kunzru, D. Saraf and S. K. Gupta, *Ind. Eng. Chem. Res.*, **41**, 4765 (2002).
32. J. Souza, J. Vargas, O. Von Meien, W. Martignoni and J. Ordonez, *J. Chem. Technol. Biotechnol.: Int. Res. Process, Environ. Clean Technol.*, **84**, 343 (2009).
33. E. Almeida Nt and A. Secchi, *Brazilian J. Chem. Eng.*, **28**, 117 (2011).
34. A. T. Jarullah, N. A. Awad and I. M. Mujtaba, *Fuel*, **206**, 657 (2017).
35. C. Chen, N. Lu, L. Wang and Y. Xing, *Comput. Chem. Eng.*, **150**, 107336 (2021).
36. J. Biswas and I. Maxwell, *Studies Surf. Sci. Catal.*, **49**, 1263 (1989).
37. J. Biswas and I. Maxwell, *Appl. Catal.*, **58**, 1 (1990).
38. J. Biswas and I. Maxwell, *Appl. Catal.*, **58**, 19 (1990).
39. T. Myrstad, *Appl. Catal. A: Gen.*, **155**, 87 (1997).
40. H. Gonzalez, J. Ramirez, A. Gutierrez-Alejandre, P. Castillo, T. Cortez and R. Zarate, *Catal. Today*, **98**, 181 (2004).
41. K.-H. Lee, Y.-W. Lee, J.-D. Kim, K.-S. Jeon and B.-H. Ha, *Korean J. Chem. Eng.*, **14**, 445 (1997).
42. M. Davoodpour, R. Tafreshi, A. A. Khodadadi and Y. Mortazavi, *Korean J. Chem. Eng.*, **34**, 681 (2017).
43. J. S. Magee and M. M. Mitchell, *Fluid catalytic cracking: Science and technology*, Elsevier (1993).
44. J. L. Fernandes, J. J. Verstraete, C. I. Pinheiro, N. M. Oliveira and F. R. Ribeiro, *Chem. Eng. Sci.*, **62**, 1184 (2007).
45. C. Daly, N. Tidjani, G. Martin and J. Roesler, *Détermination des paramétres cinétiques dans la régénération des catalyseurs de FCC*, Technical Report No. 56010, Institut Français du Pétrole (2001).
46. M. Zwinkels and L. Nougier, *FCC regenerator simulation model*, Technical Report No. 44143, Institut Français du Pétrole (1997).
47. G. Wang, S. Lin, W. Mo, C. Peng and G. Yang, *Ind. Eng. Chem. Process Des. Dev.*, **25**(3), 626 (1986).
48. B. Alsadik, *Adjustment models in 3D geomatics and computational geophysics: With MATLAB examples*, Elsevier (2019).
49. D. Pugliese, F. Bella, V. Cauda, A. Lamberti, A. Sacco, E. Tresso and S. Bianco, *ACS Appl. Mater. Interfaces*, **5**, 11288 (2013).

50. S. Galliano, F. Bella, M. Bonomo, F. Giordano, M. Grätzel, G. Viscardi, A. Hagfeldt, C. Gerbaldi and C. Barolo, *Xanthan-based hydrogel for stable and efficient quasi-solid truly aqueous dye-sensitized solar cell with cobalt mediator*, Solar Rrl, 2000823 (2021).

APPENDIX

The reaction rate of each lump in the riser is calculated by Eq. (33):

$$r_i = \sum_j r_{ji} - \sum_j r_{ij} \tag{33}$$

where r_{ji} and r_{ij} are, respectively, the rate of reaction of lump j toward lump i and the rate of reaction of lump i toward lump j.

The multiplication of mean density and mean specific het capacity is calculated from Eq. (34):

$$\rho_m C_{p_m} = \varepsilon_g \rho_g C_{p_g} + \varepsilon_c \rho_c C_{p_c} \tag{34}$$

Gas and catalyst volume fractions in the riser are calculated from Eq. (35) to Eq. (39):

$$\varepsilon_g = \frac{F_{tf}/\rho_{ov}}{(F_{tf}/\rho_{ov} + F_{rc}/\rho_c)} \tag{35}$$

$$\varepsilon_c = 1 - \varepsilon_g \tag{36}$$

$$r_c = (V_{dry} + V_{wet}) Y_C \tag{37}$$

$$V_{dry} = k_{C1}^{dry} \exp\left(-\frac{E_{C1}^{dry}}{RT}\right) P_{O_2}^{0.78} \tag{38}$$

$$V_{wet} = k_{C1}^{wet} \exp\left(-\frac{E_{C1}^{wet}}{RT}\right) \frac{P_{H_2O} P_{O_2}^{0.84}}{P_{O_2}^{0.84} + k_{C2}^{wet} \exp\left(-\frac{E_{C2}^{wet}}{RT}\right) P_{H_2O}} \tag{39}$$

The subscripts "dry" and "wet" represent the partial contributions due to dry and wet conditions during coke combustion.

Pressure balance calculated from Eq. (40):

$$\frac{\partial P_{LF}}{\partial z} = -(\varepsilon_{cLF}\rho_c + \varepsilon_{gLF}\rho_{gLF})g \tag{40}$$

Volume fractions of gases and the catalyst are calculated by Eq. (41) and Eq. (42) [24]:

$$\varepsilon_g = 1 - \frac{2.06 G_c \exp(0.251 u_g)}{\rho_c} \tag{41}$$

$$\varepsilon_c = 1 - \varepsilon_g \tag{42}$$

Gas superficial velocity and the catalyst mass flux are calculated from Eq. (43) and Eq. (44):

$$u_g = \frac{F_g}{\rho_g A_{LF}} \tag{43}$$

$$G_c = \frac{F_c}{A_{LF}} \tag{44}$$

The volume of the dense bed is calculated from Eq. (45):

$$V_{bed} = L_{RG} A_{RG} \tag{45}$$

Volume fractions of gases and the catalysts are calculated from Eq. (46) and Eq. (47):

$$\varepsilon_{gRG} = \frac{u_{gRG} + 1}{u_{gRG} + 2} \tag{46}$$

$$\varepsilon_{cRG} = 1 - \varepsilon_{gRG} \tag{47}$$

The superficial velocity in dense bed phase is calculated from Eq. (48) and Eq. (49):

$$u_{gRG} = \frac{F_{gRG}}{\rho_{gRG} A_{RG}} \tag{48}$$

$$H_k = C_{p_k}(T_k - T_{ref}) \tag{49}$$

Weight fraction of the coke in the lift section is calculated by Eq. (50) to Eq. (52):

$$Y_{ckRG} = Y_{C,\,RG} + Y_{H,\,RG} \tag{50}$$

$$Q_r^0 = V_{bed}\left(\varepsilon_{gRG}\sum_j r_j^g \Delta H_j^g + \varepsilon_{cRG}\rho_c \sum_j r_j^s \Delta H_j^s\right) \tag{51}$$

$$Q_{loss} = \pi D_{RG} L_{RG} U_{RG} (T_{surr} - T_{RG}) \tag{52}$$